Interactions of Two Monoclonal Antibodies with BNP: High Resolution Epitope Mapping Using Fluorescence Correlation Spectroscopy

Sergey Y. Tetin,*,‡ Qiaoqiao Ruan,‡ Sylvia C. Saldana,‡ Mark R. Pope,§ Yan Chen,‡ Huaiqin Wu,‡ Mary S. Pinkus,‡ Jianjun Jiang,|| and Paul L. Richardson||

Biotechnology and Process Design, Core Research and Development, Diagnostics Division and Advanced Technology, Global Pharmaceutical Research and Development, Abbott Laboratories, Abbott Park, Illinois 60064

Received April 11, 2006; Revised Manuscript Received July 24, 2006

ABSTRACT: Structure−function studies of antibody−antigen systems include the identification of amino acid residues in the antigen that interact with an antibody and elucidation of their individual contributions to binding affinity. We used fluorescence correlation spectroscopy (FCS) and alanine-scanning mutagenesis to characterize the interactions of brain natriuretic peptide (BNP) with two monoclonal antibodies. Human BNP is a 32 amino acid residue long cyclic polypeptide with the ring structure confined between cysteines in positions 10 and 26. It is an important cardiovascular hormone and a valuable diagnostic cardiac marker. We compare the binding strength of the *N*-terminus Alexa488-labeled BNP, native cyclic BNP, BNP alanine-substituted mutants, linear BNP, and its short fragments to determine the individual contributions of amino acid residues included in the continuous antigenic epitopes that are recognized by two different monoclonal antibodies raised toward BNP. Implementation of FCS for these studies offers all of the advantages of solution phase measurements, including high sensitivity, simplicity of manipulation with reagents, and elimination of solid phase interferences or separation steps. Significant differences in the molecular masses of the free and antibody bound BNP results in a substantial (∼2.5-times) increase in the diffusion rates. Determination of the binding constants and inhibition effects by measuring the diffusion rates of the ligand at the single molecule level introduces the ultimate opportunity for researching systems where the fluorescence intensity and/or fluorescence anisotropy do not change upon interaction of the ligand with the protein. Monoclonal antibodies 106.3 and BC203 demonstrate high affinities to BNP and bind two distant epitopes forming robust antibody sandwiches. Both antibodies are used in Abbott diagnostic assays on AxSYM, IMx, and Architect platforms.

Determination of antigenic regions (epitopes) in peptides and proteins is an important step in the structure−function characterization of antibody−antigen systems. These regions are involved in immediate interactions with amino acid residues in the antibody binding site and are characteristic of a specific antibody. Understanding the contribution of each residue in the epitope to the strength of the antibody−antigen interaction uncovers the binding mechanism and facilitates possible improvements of the antibody via protein engineering.

Brain natriuretic peptide (BNP), often referenced as the B-type natriuretic peptide, is an important cardiovascular hormone that participates in the regulation of sodium and water excretion, that is, natriuresis. Along with two other natriuretric peptides, the atrial natriuretic peptide (ANP) and the C-type natriuretic peptide (CNP), it belongs to the natriuretic peptide hormone family (*1*). BNP was first isolated from the porcine brain and named accordingly (*2*). Regardless of its confusing name, BNP is a cardiac hormone that is synthesized predominantly in the heart ventricles (*3*), whereas ANP is secreted into the blood stream from the heart atria (*4*−*6*), and CNP is mainly produced by endothelial cells in the brain (*7*). Natriuretic peptides act through the pertinent guanylyl-type membrane bound receptors (*8*−*10*). They can be also eliminated from circulation by another, clearance-type receptor, which is not coupled to guanylate cyclase and is probably not accountable for any other physiological function (*10*−*12*).

All natriuretic peptides are synthesized in longer pro-hormone form and activated by limited proteolysis. For instance, BNP is cleaved from the *C*-terminal portion of the 134-amino acid pro-BNP (*13*). Secretion of ANP and BNP can be enhanced by stretching the atria or ventricles, respectively, and will result in an increase in natiuresis, vasodilatation, inhibition of the renin−angiotensin−aldosterone activity, and suppression of the sympathetic nervous system (*14*). Numerous contemporary reviews on physiology of natriuretic peptides and their role in illness can be found elsewhere (*14*−*16*). A recombinant BNP, named *Nesiritide*, has been recognized as an efficient drug for the treatment of heart failure (*17*, *18*).

Another aspect of BNP's clinical importance pertains to its role as a valuable diagnostic cardiac marker (*19*). It has been proven that elevated levels of BNP or the *N*-terminal portion of pro-BNP (NT-pro-BNP) in blood plasma are reliable diagnostic indications of heart failure, and measuring the BNP concentrations in dynamics has become an impor-

* Corresponding author. Tel: 847-935-4661. Fax: 847-935-6498. E-mail: sergey.tetin@abbott.com.
‡ Biotechnology.
§ Process Design.
|| Advanced Technology.

10.1021/bi0607047 CCC: $33.50
Published on Web 11/07/2006

tant prognostic clinical test (*15*, *20*, *21*).

Natriuretic peptides are cyclic: they contain a single disulfide bond that conjoins the 17 amino acid ring. Eleven amino acids in the ring, including both cysteines, are invariant in all human or porcine natriuretic peptides. Human BNP is 32 amino acid residues long, with the ring structure confined between the cysteines in positions 10 and 26. Outside the ring, both the *N*-terminal (positions 1−9) and the *C*-terminal (positions 27−32) sequences are unique and specific to human BNP.

The three-dimensional structure of a rather short polypeptide such as BNP cannot be highly ordered. In fact, NMR studies of the porcine BNP in dimethylsulfoxide (*22*, *23*) and in water (*24*) indicated variations in the conformation of this peptide. Similar studies of ANP (*25*, *26*) also did not show a well-defined secondary structure, though revealing some ordered regions. Notably, receptor bound ANP attained binding induced conformation (*9*, *27*).

On the basis of these observations, it is rational to suggest that antibodies toward BNP would likely recognize linear, conformation independent antigenic determinants (epitopes), and the interaction of BNP with antibodies should follow the induced fit binding mechanism. The structural malleability of BNP readily permits the use of short peptides that represent BNP fragments for the determination of the epitope. It also enables the application of the powerful alanine scanning approach for the elucidation of the contribution of each amino acid residue within the epitope to the strength of antibody−BNP binding. This method was originally introduced for epitope scanning in human growth hormone (*28*) and quickly became a versatile strategy for fine epitope mapping.

In addition to a significant theoretical interest inherent to antibody−peptide systems, the precise determination of BNP antigenic epitopes directly relates to practical selection of antibodies for quantitative immunoassays. It is critical for the understanding of their fine specificity and capability to recognize products of BNP proteolytic degradation in the patient plasma.

High-resolution mapping of antigenic epitopes requires sensitive and rigorous detection of binding events. The implementation of fluorescence based methods for these studies offers all of the advantages of solution phase measurements, including high sensitivity, ease of manipulation with the reagents, and elimination of any solid phase artifacts or separation steps (*29*). However, such methods require the careful incorporation of a brightly fluorescent reporter group into at least one of the reagents. We chose to specifically tether the Alexa488 dye to the BNP *N*-terminal amino group and performed appropriate controls to minimize any possible effects of the label on binding to the antibodies. Unfortunately, *N*-terminal labeling combined with BNP structural flexibility practically eliminated an opportunity to apply fluorescence quenching or fluorescence polarization based techniques. Neither of the antibodies utilized in the current study affected the fluorescence intensity of the Alexa488 labeled BNP by more than 10% or changed its anisotropy by more than 0.1. Consequently, we chose another fluorescence based method, namely, fluorescence correlation spectroscopy (FCS), which, over the past decade, has become a powerful approach for studying binding interactions at the single molecule level.

FCS enables the measurement of the diffusion rates and the number of fluorescent molecules in an open volume of solution. This elegant technique was introduced more than 30 years ago (*30*, *31*) but was not frequently used until the mid 90's when faster computers and advanced instruments became available. A comprehensive overview of the FCS basic principles and applications can be found elsewhere (*32*, *33*). FCS has been successfully used for the detection of antibody−antigen complexes (*34*) and the determination of antibody binding constants in solution (*35*); the general problems related to these experiments were recently reviewed (*36*).

In this article, we use FCS to compare the binding strength of BNP and related peptides to determine individual contributions of amino acid residues included in the continuous antigenic epitopes that are recognized by two different monoclonal antibodies raised toward BNP. A significant difference in the molecular mass of the free and antibody bound BNP results in a substantial, approximately 2.5-times, increase in the diffusion rate, facilitating the analysis of the FCS data.

MATERIALS AND METHODS

Antibodies. The murine hybridoma cell line producing mAb 106.3 (IgG1, κ) was obtained from Scios, Inc. (Mountain View, CA) (*37*). The cells were grown using serum free media. The antibody was purified from the media using rProtein-A Sepharose Fast Flow (Pharmacia AB, Amersham Biosciences, Piscataway, NJ) by standard procedure. Purified mouse mAb BC203 (IgG1, κ) was purchased from Shionogi & Co., Limited (Osaka, Japan) (*38*). Purity of all antibody preparations was confirmed by SDS−PAGE analysis. Antibody concentrations were determined by UV absorption in a 1 cm cuvette using $E_{279}^{1\ mg/mL} = 1.50$ or $\epsilon_{279}^{M} = 150\ 000\ M^{-1}\ cm^{-1}$ on a Cary 4 spectrophotometer (Varian, Sugarland, TX), with corrections included for scattered light.

BNP and Other Peptides. High purity cyclic BNP (M.W. = 3464) was purchased from Peptide Institute, Inc. (Osaka, Japan) as a lyophilized powder.

Alexa488 labeled BNP, referenced further in this article as the tracer, was made by selective coupling of the Alexa488 succinimidyl ester (Molecular Probes, Inc., Eugene, OR) to the *N*-terminal amine of BNP (American Peptide Company, Sunnyvale, CA) at pH 6.0. The uncoupled dye was removed on a G-25 column equilibrated with 0.01 M phosphate buffer at pH 7.4 containing 0.15 M NaCl (PBS). The tracer was further purified on a reverse-phase HPLC system running Unipoint software (Gilson, Inc., Middleton, WI) and equipped with a 25 × 200 mm radial compression column containing Delta-Pak C_{18} packing (Waters, Inc., Taunton, MA). A linear gradient of 0.1% trifluoroacetic acid/water and acetonitrile was used for elution. The identity and purity (>90%) of the final product was confirmed by mass spectrometry and reverse-phase analytical HPLC on a 4.6 × 250 mm YMC ODS-AQ, 5 μm, 120 Å column (Waters, Inc.) connected to a Hewlett-Packard 1050 series system equipped with diode-array UV−Vis and fluorescence detectors (Agilent Technologies, Palo Alto, CA) and using a linear gradient of 0.1% trifluoroacetic acid/water and acetonitrile.

Two fluorescently labeled short peptides, 6-Alexa488-BNP(5−13, C10A) and Oregon Green 488-Ala-BNP(27−

32), were prepared by reacting the succinimidyl ester of Alexa488 or Oregon Green 488 (Molecular Probes, Inc.) with the *N*-terminal amine of each peptide in anhydrous DMSO containing 1% (v/v) diisopropylethylamine followed by purification by RP-HPLC as described for Alexa488 labeled BNP.

Linear BNP 1-32 (no disulfide bond), and six BNP alanine-substituted mutants, BNP K27A, V28A, L29A, R30A, R31A, and H32A, were assembled on a Pioneer automated synthesizer (Applied Biosystems) using the manufacturer's suggested coupling protocols and reagents. Following cleavage (*39*) and precipitation with diethylether, the peptides were either cyclized with potassium ferricyanide prior to purification (*40*) or directly purified and validated as described for the tracer.

Short peptides *N*-acetyl-BNP(5-13)-carboxylamide, NH_2-BNP (5-13, C10A), NH_2-Ala-BNP(27-32), and one of the BNP alanine-substituted mutants (BNP G25A) were assembled on a 433A automated synthesizer (Applied Biosystems, Foster City, CA) using standard Fastmoc deprotection/coupling cycles.

The following BNP alanine substituted mutants were purchased from American Peptide Company: D16A, R17A, I18A, S19A, S20A, S21A, S22A, G23A, and L24A. The truncated *N*-acetyl-BNP(24-32)-carboxylamide, *N*-acetyl-BNP(4-15)-carboxylamide and its alanine-substituted derivatives, M4A, V5A, Q6A, G7A, S8A, G9A, F11A, G12A, R13A, K14A, and M15A, were purchased from AnaSpec, Inc. (San Jose, CA). The molecular weights of all BNP lots, labeled BNP derivatives, and all other peptides were confirmed by matrix-assisted laser desorption/ionization time-of-flight mass spectrometry (MALDI-TOF-MS).

All peptides utilized in this study were soluble in water or PBS. Concentrations of the peptides were assigned on the basis of their dry weight measured before dissolving or assigned by the manufacturer.

FCS Instrument and Data Analysis. FCS experiments were performed using a dual-channel fluorescence correlation spectrometer ALBA (ISS, Champaign, IL) integrated with an inverted Nikon Eclipse TE300 fluorescence microscope (Nikon InsTech Co., Ltd., Kanagawa, Japan).

A mode-locked Tsunami titanium-sapphire laser pumped with a 5 W Millennia VIs (Spectra-Physics, Mountain View, CA) was used as a two-photon excitation light source. Tsunami operates at 80 MHz with a 100-fs pulse width and is tunable between 700 and 1000 nm. The laser beam is expanded with a High Laser Beam Expander HB-4X-AR.16 coated for the 650−1000 nm region (Newport Corp., Irvine, CA) to overfill the back aperture of a Nikon Plan Apo 60X/1.2W objective, creating a diffraction limited focal spot.

A dichroic mirror (700DCSPXR, Chroma Technology Corp., Rockingham, VT) is installed in the microscope to direct the excitation beam to the sample and the emission fluorescence light to the detector(s). In addition, a band pass filter (E700sp-2p, Chroma Technology) is placed before the detectors to further reduce any leakage of the excitation light.

The size of the excitation volume was calibrated using an analytically prepared 35 nM solution of Rhodamine110 (Molecular Probes, Inc.). The autocorrelation curve calculated from the FCS data was fitted with the single component model and the Rhodamine110 diffusion coefficient equal to 270 $\mu m^2/s$. Typically, the resulting ω_0 value and the Z_0/ω_0 ratio were 0.3 μm and 4, respectively.

FCS data were initially processed with Vista (version 3.36) FCS software (ISS) using the intensity autocorrelation function to calculate the autocorrelation curve. Further analysis was performed with Globals Unlimited software (*41*) (Laboratory for Fluorescence Dynamics, Urbana, IL) to calculate the fraction of each species, the diffusion rates, and associated errors.

Steady-State Fluorescence Measurements. These measurements were performed on an SLM 8100 photon counting spectrofluorimeter equipped with prism polarizers.

Kinetics Measurements. The on-rate of mAb 106.3 was determined using a BioLogic stopped-flow module SFM-3 mounted on an SLM-Aminco AB-2 fluorimeter. Because binding to the mAb 106.3 resulted in a pronounced quenching of the labeled peptide's fluorescence, the fluorescence-quenching effect was used to monitor the binding kinetics. The association curve was collected 10 times, averaged, and fit to the pseudo-first order rate equation (*42*). The off-rate was measured using an SLM 8100 spectrofluorimeter. The simple first-order kinetics model was also used to calculate the k_{off} value.

All binding measurements were performed in 10 mM HEPES buffer at pH 7.4, containing 0.15 M NaCl, 3 mM EDTA, and 0.005% surfactant P20.

Direct Binding Experiments. In these measurements, the tracer concentration was kept constant at or below the dissociation constant value, whereas the antibody concentration was incrementally increased from the subnanomolar to micromolar range in the series of 14 samples. Samples were placed into a Lab-Tek eight chambered coverglass or 96 microwell optical bottom plates (Nalge Nunc International Corp., Rochester, NY). The excitation wavelength was set at 780 nm with a power of 3 mW on the sample. The sampling rate was set at 200 kHz, and 10 million points were collected for every measurement. Each sample was measured twice, and the autocorrelation curves were fit using the two-component autocorrelation function model with Globals Unlimited (*41*). First, the diffusion coefficients of the free and antibody-saturated tracer were measured. Then, we measured all samples in the titration series and processed the data by setting the diffusion coefficients for the free and antibody bound tracer at fixed values and varying the fractions of each component. Assuming that the fraction of the slow-diffusing component can be directly translated into the fraction of the bound tracer (F_b), the concentration of the free antibody binding sites can be calculated from the following formula:

$$S_{free} = S_{total} - T_{total} \times F_{slow} \quad (1)$$

where S_{total} and T_{total} are the antibody binding sites and total concentrations of the tracer, respectively, S_{free} is the free antibody binding site concentration, and F_{slow} is equal to F_b. Then, the binding data were fit with the simple binding model:

$$F_b = \frac{S_{free}}{K_d + S_{free}} \quad (2)$$

where K_d is the equilibrium dissociation constant. Corrections

for a relatively small fraction of the doubly liganded IgG present at the middle of the titration series (*36*) did not measurably affect the calculations of K_d.

All binding plots in this article were generated using the program Origin (OriginLab, Northampton, MA).

Competitive Binding Experiments. Solutions containing 3 or 4 nM Alexa488-BNP tracer and antibody were prepared at the concentration that is sufficient to bind approximately 90% of the tracer. Serially diluted solutions of the inhibitor (alanine substituted BNP mutants, linear BNP, short peptides, or unlabeled full length cyclic BNP) were made and added to the BNP tracer−antibody mixture for overnight incubation at room temperature. Then, samples were measured using FCS. Inhibition or the increase in fraction of the free (displaced) tracer was plotted as a function of the total inhibitor concentration.

None of the antibodies used in this study changed the fluorescence intensity or anisotropy of the tracer's reporter group. Thus, we assumed that selective labeling of the full length cyclic BNP with Alexa488 at the *N*-terminus does not affect its binding to the antibodies, and the dissociation constants are the same for the unlabeled and labeled antigen. The fraction of the tracer (F_{free}) displaced by the inhibitor can be calculated from the following equation:

$$F_{free} = [I_{total} + T_{total} - S_{total} - K_d + \sqrt{(S_{total} + I_{total} + T_{total} + K_d)^2 - 4 \times S_{total} \times (I_{total} + T_{total})}]/[2 \times (I_{total} + T_{total})] \quad (3)$$

where I_{total}, T_{total}, and S_{total} are the total concentrations of inhibitor, tracer, and antibody binding sites, respectively, and K_d is the dissociation constant similar for the tracer and inhibitor. Equation 3 was derived for the case when $K_d = K_i$ from the formulas defining dissociation constants:

$$K_d = \frac{T_{free} \times S_{free}}{T_{bound}} \text{ or } K_i = \frac{I_{free} \times S_{free}}{I_{bound}}$$

and the mass conservation law:

$$T_{total} = T_{free} + T_{bound}$$
$$I_{total} = I_{free} + I_{bound}$$
$$S_{total} = S_{free} + S_{bound}$$

Equation 3 was used to evaluate the displacements of the tracer with the full length cyclic BNP (corresponding plots in Figures 2 and 5) and to fit data presented in Figure 3.

However, if $K_i \neq K_d$, eq 3 becomes inapplicable, and all other plots in Figures 2 and 5 are shown only for apparent comparison. For a more rigorous evaluation, they should be treated using a cubical polynomial (*43*).

RESULTS

Determination of the Diffusion Coefficients in FCS Experiments. FCS is a powerful and reliable method to measure the diffusion rates of molecules. Differences in the size of the free and antibody bound Alexa488-BNP tracers permitted reasonable separation of these two diffusing species. However, as with any other technique, FCS experiments require careful execution and data evaluation. In this short section, we will address the most important experimental details that must be considered when performing FCS.

Several potential issues, such as excitation saturation, photo bleaching, binding induced quenching, and high background fluorescence, are related to the properties of the sample. The level of the excitation power may affect FCS results because of the saturation of the fluorescence excitation, thereby altering the size and shape of the observation volume in which fluorescence fluctuations are monitored (*44*). As a commonly practiced prevention of this effect, we produced a power plot (for two-photon excitation, it is a plot of square root of the fluorescence intensity as a function of the laser power) for the Alexa488-BNP tracer and found that it is linear for the power levels on the sample under 4 mW. Thus, the 3.0−3.5 mW power range was used in all our experiments.

Another problem that relates to the excitation power is the photo bleaching of the sample. Apparently, the slow-diffusing species is more susceptible to bleaching because slow-diffusing molecules remain longer in the excitation volume. We did not see photo bleaching in any of the experiments presented here, and as an example, in the insert in Figure 1B, we show that the intensity of the antibody bound Alexa488-BNP tracer did not change in the course of the experiment. The diffusion coefficients of the antibody−tracer complexes measured at two power levels of 2 mW and 3.5 mW were the same.

Binding induced quenching of the fluorescent probe should be also considered in FCS data analysis because in this situation, the contributions of the free and bound tracer molecules to the auto correlation function curves are different (*36*). It is important to indicate that in the current study, the Alexa488-BNP tracer was intentionally prepared by selective coupling of the dye to the *N*-terminal amine of the peptide. Therefore, there was no significant quenching of the tracer fluorescence observed upon its interaction with either antibody under study. As follows from the intensity data mentioned in the caption to Figure 1, the saturation of the Alexa488-BNP tracer with mAb BC203 and mAb 106.3 resulted in a mere 3% and 8% quenching, respectively.

Background fluorescence is a common obstacle in any fluorescence measurement when approaching low tracer concentrations. In our experiments, it was on the order of 300 counts/s, whereas the fluorescence intensity of the tracer was at least 10 times higher. However, it limited further dilutions of the tracer in the binding experiments with mAb 106.3 presented in Figure 1B. Decreasing the concentration of the Alexa488-BNP tracer below 1 nM did not permit a reliable fit of the auto correlation plot into two components.

Other important experimental problems, such as poor signal-to-noise ratio, insufficient sampling, and associated bias, are related to the instrumentation and experimental conditions. General statistical analysis of the FCS data, including analytical derivation of standard deviations and calculations of the noise, signal-to-noise ratio, and bias, was comprehensively discussed by Saffarian and Elson (*45*).

Both insufficient sampling rate (undersampling) and inadequate data acquisition time may lead to a bias in FCS measurements. This happens when the diffusion rate of the fluorescent molecules or their complexes is faster or comparable to the sampling rate. It was controlled in our measurements by keeping the sampling rate at 5 μs, which is much shorter than the 100 μs diffusion rate of the free tracer.

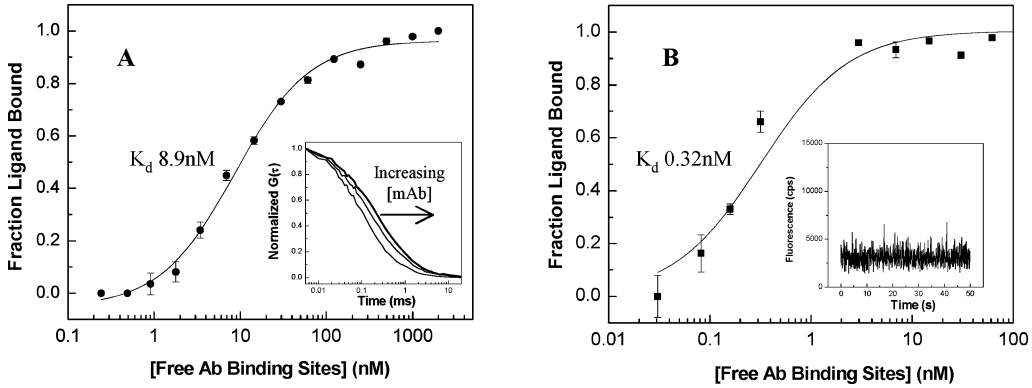

FIGURE 1: Determination of the dissociation constants of the Alexa488-BNP tracer and monoclonal antibodies. Fraction of the bound tracer was assumed to be equal to the fraction of the slow-diffusing species calculated from the two-component fit of the autocorrelation curves. During fitting, the diffusion coefficients of the free and antibody saturated tracers were fixed as 110 $\mu m^2/s$ and 45 um^2/s, respectively. The error bars at each point show the uncertainty of the calculated values. The concentrations of the free antibody binding sites along the titration series were calculated from the eq 1, and the dissociation constants were obtained from the fit using the simple binding model, eq 2. (A) Binding curve of the BNP tracer and mAb BC203. The concentration of the tracer was kept constant at 2 nM. Fluorescence of the free Alexa488-BNP was 6100 counts/s, whereas the fluorescence of the antibody saturated tracer was 5900 counts/s. A K_d of 8.9 ± 1.0 nM was determined from the fit. The insert shows the autocorrelation function curves (ACF) of the free, partially bound, and completely saturated Alexa488-BNP tracers. At the intermediate antibody concentrations, the tracer is partially saturated with the antibody, yielding two components in the ACF curve. (B) Binding curve of the Alexa488-BNP tracer and mAb 106.3. The concentration of the tracer was kept constant at 1 nM. Fluorescence of free Alexa488-BNP was 3700 counts/s, and the fluorescence of the antibody saturated tracer was 3400 counts/s. Further dilution of the tracer was restricted by measurable background fluorescence (300 counts/s). The estimated K_d is 0.32 ± 0.09 nM. The insert shows that the intensity of the antibody bound Alexa488-BNP tracer did not change during the course of the experiment.

The signal-to-noise ratio in FCS experiments can be estimated by using the phase diagram published by Saffarian and Elson (*45*). It was 100:1 or better in all our measurements, which translated into rather small standard deviations of the calculated diffusion coefficients.

The diffusion coefficient and $g(0)$ of each component as well as associated standard deviations were calculated using Globals Unlimited software. The $g(0)$ values show the fractional intensities of each diffusing species, and the ratio $g(0)_{slow}/[g(0)_{slow} + g(0)_{fast}]$ can be directly translated into the fraction of bound ligand (*36*). The standard deviations of $g(0)$ values calculated by the Globals software are shown as errors of the fraction of bound ligand in the Figures or mentioned in related captions. It is important to indicate again that this analysis was simplified because neither of the antibodies under study quenched the Alexa488-BNP tracer.

In all experiments, this error was less than 3% for the fraction bound of 0.5 or higher. However, in the beginning of the titration, the errors in the measured fraction bound are typically higher. For example, the standard deviation of ±9% was calculated for the first several points in the experiment presented in Figure 1B.

Rather small standard deviations in our FCS data were also confirmed by direct determination of the experimental error. The standard deviations calculated for the diffusion coefficient and $G(0)$ obtained in 30 repeated measurements of a 3 nM tracer solution were ±2.6% and ±1.3%, respectively.

As determined, the diffusion coefficient of the free Alexa488-BNP tracer is 110 ± 3 $\mu m^2/s$. The diffusion coefficient of the tracer bound to either antibody under study is 45 ± 1 $\mu m^2/s$.

Determination of the Dissociation Constants. The dissociation constants (K_d) of the tracer with both anti-BNP antibodies were measured in direct binding experiments. Figure 1 shows examples of the autocorrelation function curves and binding plots for the antibodies under evaluation. For mAb BC203, the dissociation constant of 8.9 ± 1.0 nM was calculated from the fit.

Because of its higher affinity, the binding experiment with mAb 106.3 required lower concentrations of the tracer solution. However, dilution of the tracer to concentrations under 1 nM was limited by considerable background fluorescence (300 counts/s), which complicated the two-component fit of the autocorrelation function. Thus, the concentration of the tracer in this experiment was kept at 1 nM. Consequently, it led to noticeable stoichiometric characteristics in the binding plot and a relative increase in the error of the estimated K_d (0.32 ± 0.09 nM). Later on, we will describe further verification of this dissociation constant.

The dissociation constants obtained in these direct binding experiments were applied to calculations of the antibody and BNP tracer concentrations to prepare tracer−antibody complexes for further competitive binding experiments.

Determination of the BNP Epitopes by the Alanine Scan Approach. The purpose of these competitive binding experiments was to determine amino acid residues in the BNP molecule that are critical for its recognition by each of the antibodies. The Alexa488-BNP tracer and antibody were initially mixed as described below, and the alanine-substituted BNP mutants were added at various concentrations for overnight incubation. The autocorrelation curves were measured for each sample using full length cyclic BNP as the control. Peptides, containing mutations that do not affect their ability to interact with antibodies, displaced the BNP tracer at the same concentrations as native BNP.

While working with mAb 106.3, we kept the concentration of the labeled BNP at 3−4 nM and saturated it to approximately 90% with 8−10 nM antibody. The theoretical concentration of the inhibitor (unlabeled BNP) calculated

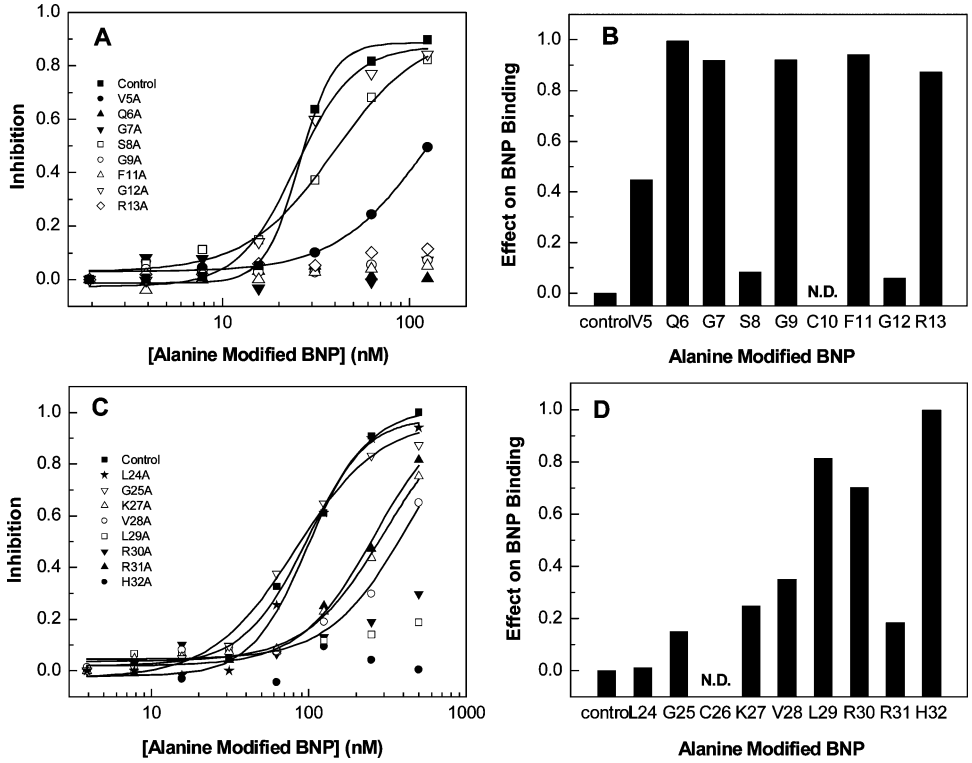

FIGURE 2: Competitive displacement of the Alexa488-BNP tracer by the alanine substituted BNP mutants. (A, B) The Alexa488-BNP tracer (3 nM) is premixed with mAb 106.3 (8 nM) and (C, D) the Alexa488-BNP tracer (4 nM) is premixed with mAb BC203 (30 nM). Left panels show the actual data points, and the relative effects of each alanine substitution on the antibody−BNP interaction are shown in the right panels. The standard deviations at points above 50% inhibition were less than ±8%. Mutations outside of the shown epitope sequences did not affect the competition and, therefore, were excluded from the Figures.

using eq 3, which should displace 80−85% of the tracer at these experimental conditions, is 100 nM, which is in a good agreement with the data (Figure 2A). Similarly, when searching for the BC203 epitope, the concentration of the BNP tracer was kept at 4 nM, but the concentration of mAb BC203 was increased to 30 nM to achieve approximately 90% saturation. In this case, the concentration of the unlabeled BNP that displaces 90% of the tracer is 500 nM. The calculated and experimental values are also in good agreement in this experimental series (Figure 2C).

BNP regions 5−13 and 27−32 were identified as the epitope areas for mAbs 106.3 and BC203, respectively. Detailed results of the competition experiments are shown in Figure 2. All other substitutions did not affect the competition and, thus, are not included in the Figure. Cysteine residues in positions 10 and 26 that confined the BNP ring were not mutated in these experiments. For each antibody, the left panel shows the inhibition as a function of mutant concentration, and the right panel demonstrates the relative effect of mutations on the binding of the BNP tracer by the antibody. The height of each bar corresponds to the inhibition at the last point of the titration. At this concentration, native BNP displaces approximately 90% of the BNP tracer from the antibody. Evidently, the effect of the substitution of individual amino acid residues in BNP with alanine is distinctive for each monoclonal antibody.

Verification of the Epitopes Using Short Linear Peptides. The epitope regions identified with alanine-scanning mutagenesis were verified in further experiments. Studying mAb 106.3, we found that the inhibition strength of the short peptide 5-13 is equal to the inhibition caused by the native

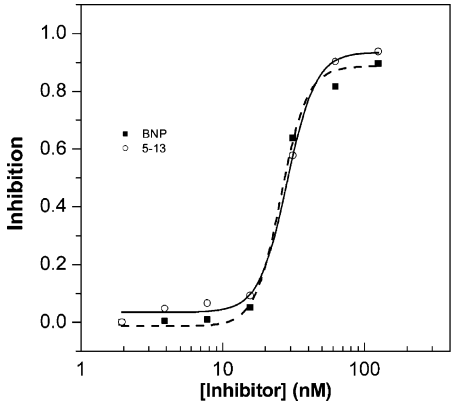

FIGURE 3: Comparison of the inhibition effects caused by the native cyclic BNP and the short peptide 5-13 on mAb 106.3. The Alexa488-BNP tracer (3 nM) is premixed with mAb 106.3 (8 nM). The standard deviations at each point in this experiment do not exceed 8%.

BNP molecule (Figure 3). Also, replacement of the cysteine at position 10 with alanine in this short peptide did not affect binding. In the case of mAb BC 203, we measured its binding to the Oregon Green−Ala-BNP(27-32) peptide and to the full length cyclic BNP tracer in a direct titration experiment and obtained similar results (Figure 4). Thus, the selected short peptides indeed represent the epitopes.

The linear full length BNP, with a reduced disulfide bond between cysteine residues 10 and 26, also demonstrated strong inhibition (Figure 5A). However, mAb BC203 binds linear BNP weaker than native cyclic BNP. Amidation of the *C*-terminal carboxyl group on histidine-32 entirely eliminates the binding of the short peptide to this antibody

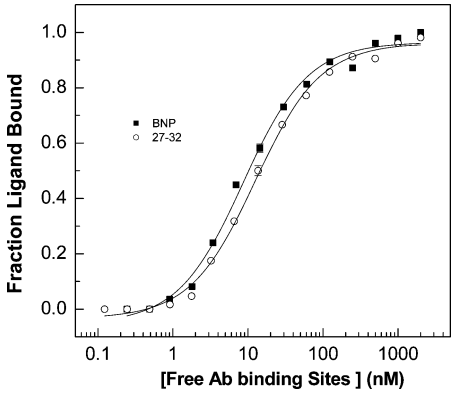

FIGURE 4: Comparison of the binding constants of the Alexa488-BNP tracer and Oregon Green-Ala-BNP(27-32) peptide with mAb BC203 in a direct titration experiment. The standard deviations at the points above 50% saturation level were less than 3% (shown in the middle of the curve) and are comparable to the symbol size. The calculated K_d values are 8.9 ± 1.0 nM and 12.5 ± 0.9 nM, and the concentrations of the Alexa488-BNP tracer and Oregon Green-Ala-BNP(27-32) peptide are 2 and 4 nM, respectively.

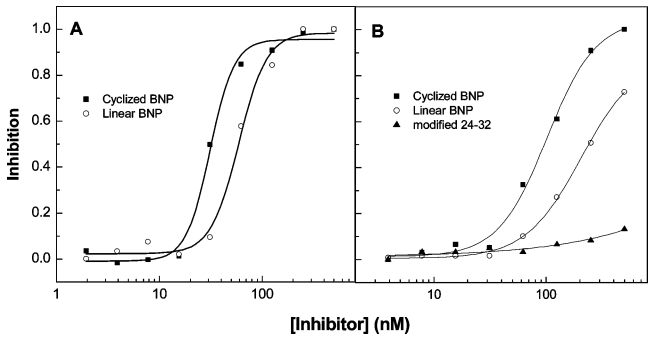

FIGURE 5: Comparison of the inhibition effects caused by the native cyclic and linear BNP on monoclonal antibodies. (A) The Alexa488-BNP tracer (4 nM) is premixed with mAb 106.3 (10 nM) and (B) the Alexa488-BNP tracer (4 nM) is premixed with mAb BC203 (30 nM). Panel B also contains the inhibition data caused by the short peptide 24-32 with the modified *C*-terminal carboxyl group (*N*-acetyl-24-32-carboxyl amine). The standard deviations at each point of the titration were less than 8%.

pointing to the critical roll of the *C*-terminus in the peptide-antibody interaction (Figure 5B).

Verification of the Dissociation Constant of mAb 106.3 Using Peptide 5-13, C10A. The fluorescence efficiency of the 6-Alexa488 labeled peptide (5-13, C10A), which completely represents the BNP binding epitope, permits its dilution to the subnanomolar range enabling high affinity measurements. As was mentioned earlier, the binding of the fluorescently labeled full length BNP tracer to either antibody used in the current study does not affect its fluorescence because the *N*-terminal location of the dye is remote from either epitope. Contrary to this construct, the Alexa488 labeled short peptide 5-13 represents the epitope, and binding to mAb 106.3 resulted in pronounced changes of its fluorescence intensity and anisotropy. In Figure 6, we show the results of the equilibrium titration experiments by means of fluorescence quenching (A) and fluorescence anisotropy (B). Both techniques produced the same dissociation constant of 0.38 ± 0.07 nM.

The K_d was also confirmed by kinetics measurements shown in Figure 6 (C and D). The association kinetics rate, k_{on}, was measured at ambient temperature by monitoring fluorescence quenching of the 6-Alexa488(5-13, C10A) peptide upon its binding to the antibody. Measurements were performed using a Biologic stopped-flow module mounted on an AB-2 fluorimeter. The binding of the peptide resulted in a monoexponential decay, and the calculated k_{on} was $3.3 \times 10^7 \pm 2.2 \times 10^5$ M^{-1} s^{-1}. The dissociation rate ($k_{off} = 1.1 \times 10^{-2} \pm 1.2 \times 10^{-4}$ s^{-1}) was calculated from the monoexponential dissociation curve when the antibody bound labeled peptide was displaced by an excess of unlabeled BNP.

Calculation of the equilibrium dissociation constant from the kinetics rates yields the K_d value of 0.33 nM, which is in good agreement with equilibrium data.

pH Dependence of BNP Interactions with Antibodies. The Alexa488-BNP complexes with mAb 106.3 or mAb BC203 were prepared in 0.l M phosphate buffer at concentrations that resulted in greater than 85% binding of the labeled peptide. The pH of the solutions was adjusted to the desired values, and after overnight incubation, all samples were measured using FCS. The results of this experiment are shown in Figure 6. Binding of BNP to mAb106.3 was not altered above pH 4 and below pH 9. The optimal pH range for mAb BC203 is narrower. The fraction of the labeled BNP bound to this antibody decreases when approaching pH 5 and 8, indicating dissociation of the complex.

DISCUSSION

FCS has become a powerful method for studying binding interactions in solution (*33*, *36*). Determination of the binding and inhibition constants by measuring the diffusion rates of the ligand at the single molecule level introduces the ultimate opportunity for researching systems where the binding-induced changes in fluorescence intensity or anisotropy are absent. With the objective of minimizing possible interactions of the label with the antibodies, we selectively coupled the full length BNP with the dye at the *N*-terminal amino group that is distant from both described epitopes.

As demonstrated in the current study, determination of the binding constants and inhibition effects by FCS in the solution phase is reasonably simple, especially when the free and antibody bound ligands demonstrate significant differences in the diffusion rates. However, several important issues related to the photo characteristics of the sample as well as the instrumentation and experimental conditions should be carefully considered when performing FCS (*44*, *45*). Sample related problems such as excitation saturation, photo bleaching, binding induced quenching, background fluorescence, and matters associated with the experimental conditions, including poor signal-to-noise ratio, insufficient sampling, and associated bias, have been addressed earlier in this article. Keeping the instrument alignment consistent and performing thorough calibration assures high day-to-day reproducibility of the FCS results.

Generally speaking, we are convinced that in solution-phase experiments, preparation and titration of the samples introduces more uncertainties into binding constant determinations than FCS measurements per se. Treating the titration series as a specific data set and performing a global fit of the data minimizes experimental error.

Alanine-scanning mutagenesis was introduced and successfully utilized for discovering the receptor-binding epitope in human growth hormone, a 22-kDa globular protein (*28*).

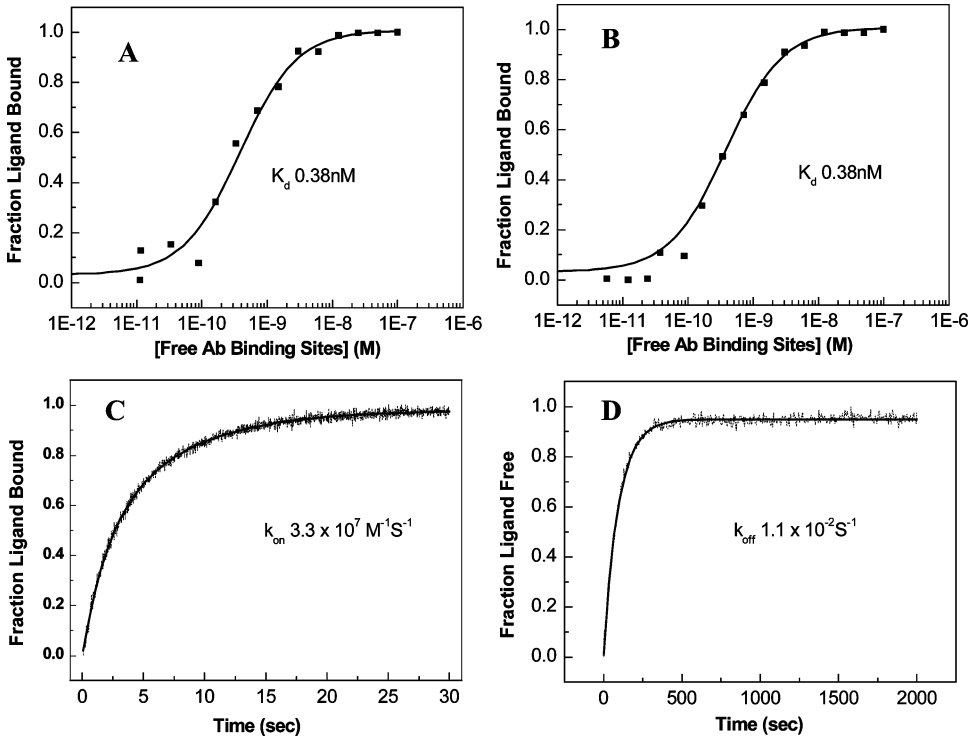

FIGURE 6: Determination of the dissociation constant of mAb 106.3 and Alexa488-BNP(5-13, C10A). The equilibrium binding curve was measured using fluorescence quenching (A) and fluorescence anisotropy (B). The K_d value is 0.38 ± 0.07 nM in both measurements. The concentration of the Alexa488-BNP(5-13, C10A) peptide is 0.05 nM. (C) The association kinetics curve: the final concentrations of the Alexa488-BNP(5-13, C10A) peptide and mAb 106.3 were 10 and 5 nM, respectively. The same on-rate values ($3.3 \times 10^7 \pm 2.2 \times 10^5$ M^{-1} s^{-1}) were also determined using 10 and 15 nM solutions of mAb 106.3. (D) The dissociation kinetics curve measured by a 100-fold dilution of the 5 nM antibody−peptide stoichiometric complex into a 10 nM solution of the unlabeled native BNP to prevent the association reaction. The off-rate is $1.1 \times 10^{-2} \pm 1.2 \times 10^{-4}$ s^{-1}. The experiment was also reproduced with 7.5 and 15 nM unlabeled BNP. The K_d value calculated using the kinetics rates is 0.33 nM.

The combination of the alanine-scanning approach with the complementary homologue-scanning mutagenesis (*46*) diminishes the potential misinterpretation of the consequences of alanine substitution caused by remote effects of the mutation via protein conformation. Interpretation of the alanine-scanning results is easier when working with peptides that do not have a highly ordered 3D structure. In these situations, the probability that the alanine substitution affects the peptide conformation is minimal. As we indicated earlier, BNP in solution is highly flexible and adjusts to multiple conformations (*22*, *23*), which largely substantiates the application of the alanine-scanning tool for the purpose of the current study. The ability to define the epitope using this tool and then to replicate it solely with a short peptide (Figures 3 and 4) confirms the absence of the conformation mediated effects of alanine substitutions.

However, the presence of the disulfide bond that causes the cyclic nature of all natriuretic peptides partially restricts the mobility within the confined ring and limits the number of possible BNP conformations in solution as demonstrated by NMR (*22*, *24*). For both studied antibodies, the linear full length peptide construct caused less inhibition than native cyclic BNP or the short "antigenic epitope" peptide (Figure 5), suggesting that a considerable fraction of the linear full length BNP derivative remains in a conformation that masks the epitope and is unfavorable for antibody recognition.

Studying mAb 106.3−BNP complexes by alanine-scanning mutagenesis, we identified nine BNP amino acids in positions 5−13, which when replaced with alanine altered the binding. The sequence of the identified epitope is consistent with previously published data (*37*) and includes nine amino acids: Val_5-Gln_6-Gly_7-Ser_8-Gly_9-Cys_{10}-Phe_{11}-Gly_{12}-Arg_{13}.

On the basis of the extended length of the epitope, we can speculate that it binds in a groove shaped mouth, and both the antibody and the peptide undergo conformational adjustments, that is, binding occurs by an induced fit mechanism. Such a mechanism was previously observed in mAb BV04-01, which binds single-stranded DNA (*47*, *48*).

The relative effects of the alanine replacements on BNP binding to mAb 106.3 are shown in Figure 2. It is critical to emphasize that alanine replacements do not involve main chain carbonyl and amide groups of the peptide, probing only the involvement of side chain residues. In the case of glycines, only stereo glycines can be revealed when substituted with bulkier alanines. In BNP, Gly_7 and Gly_9 probably are such stereo glycines that provide flexibility and allow the BNP epitope to fold in the binding groove, prompting multiple peptide−antibody interactions. Replacement of either glycine with alanine strongly inhibits binding.

The side chains of three amino acids, Gln_6, Phe_{11}, and Arg_{13}, are also critical for interactions with mAb 106.3. The relatively short hydrophobic side chain of Val_5 is also important for binding but to a lesser extent. Phenylalanines and arginines are frequently included in antigenic epitopes (*49*). Both amino acids have bulky side chains and may provide multiple contacts with the antibody. Phenylalanine residues have been found in hydrophobic pockets and participate in aromatic edge-to-face or $\pi-\pi$ stacking interactions (*50*). The extended aliphatic portion of arginine is also

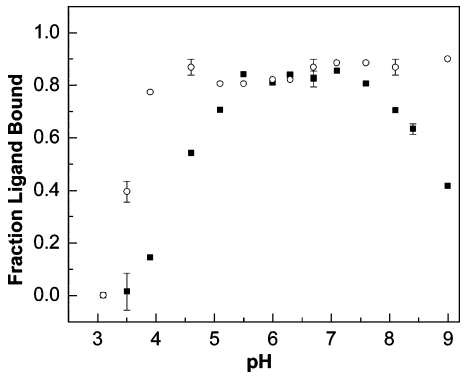

FIGURE 7: pH dependence of BNP binding to mAb 106.3 and mAb BC203. The fraction of the bound Alexa488-BNP tracer is plotted as a function of pH. Alexa488-BNP−antibody complexes were prepared to achieve 85−90% saturation of the tracer: the concentrations of Alexa488-BNP are 5 and 4nM, and the concentrations of mAb 106.3 and mAb BC203 are 15 and 25 nM, respectively. The error bars show the uncertainty of the calculated values.

often included in hydrophobic sites, and its guanidino group is the strongest positively charged group in proteins and peptides. In contrast, glutamine rarely plays a key role in antigen−antibody interactions, although it easily forms hydrogen bonds and polar contacts. On the basis of the significance of Gln_6, we can speculate that in our case, it is also a stereo residue, and its importance, at least in part, relates to the unique geometry of the complimentary site in the binding groove.

Monoclonal antibody BC203 was selected to recognize the *C*-terminus portion of BNP (*38*). The BNP epitope (Figure 2) that is recognized by this antibody includes six amino acids: Lys_{27}-Val_{28}-Leu_{29}-Arg_{30}-Arg_{31}-His_{32}.

The size and the amino acid content of the epitope are typical for immunoreactive sequences in peptides and proteins. It contains bulky residues that may participate in hydrophobic and electrostatic interactions. Three residues, Leu_{29}, Arg_{30} and, especially, His_{32}, are key amino acids in the epitope. The role of His_{32} is remarkable: both the side chain and the *C*-terminal carboxyl group are essential for the interaction with mAb BC203. Replacement of the histidine with alanine or the modification of the *C*-terminus to an amide group completely eliminates BNP reactivity with the antibody.

The extraordinary importance of His_{32} and its α-carboxyl group deserves special discussion. At pH 7.4, the predominant form of the histidine imidazolium ring is neutral, and the negatively charged α-carboxyl can make electrostatic contact with the antibody. However, it is also possible that the carboxyl anion interacts with another BNP residue, namely, the positively charged guanidino group of Arg_{30}. Because of the alternate orientation of the amino acid residues in polypeptides, the side chains of His_{32} and Arg_{30} are similarly positioned and may form an intrapeptide ion pair. This interaction is weak in solution but may become much stronger when BNP is rigidly bound in the antibody cavity. Edmundson and co-workers (*51*) described a similar mechanism that involves a histidine and the *C*-terminal *β*-alanine interaction in one of the peptides that binds to the *Mcg* L-chain dimer.

In order to test this hypothesis, we measured the pH dependence of BNP−mAb BC203 binding (Figure 7). It was altered when the pH of the buffer was below 5.5. At this pH, the histidine imidazolium ring is predominantly positively charged and can bridge with the α-carboxyl group. Thus, it may compete with the side chain of Arg_{30}, changing the BNP *C*-terminus configuration and affecting its interaction with mAb BC203. We consider this mechanism an interesting possibility requiring further confirmation by structural analysis.

Additionally, the alanine-scanning results revealed that Gly_{25} also has a small but measurable effect on the BNP−antibody interaction. It is probably another stereo residue, and its replacement with alanine influences the BNP configuration in the region adjacent to the disulfide bond and, therefore, affects the accessibility of the *C*-terminal epitope to the antibody.

In general, the induced fit mechanism, which includes both the conformational adaptation of the peptide and structural malleability of the complementary antibody binding regions, represents an interesting biophysical question. Speaking mechanistically, the antibody binding groove contains an array of interacting micro sites, each of which also binds to the corresponding array of the interacting sites on the antigen. The binding process, then, includes mutual conformational inter and intramolecular adjustments that can be synergistic, antagonistic, or neutral. These local conformational perturbations are likely cooperative, making the binding process similar to protein folding. In fact, the binding of a flexible peptide antigen in the structurally malleable groove of the antibody can be considered a reciprocally controlled folding of the peptide and the antibody complementarity determining regions (CDRs). The binding and folding processes are energetically linked. The interdependence of ligand binding and internal interactions in proteins was recognized by Wyman (*52*, *53*) and further elaborated by Weber, who introduced the terms of micro and macro associations in proteins and formulated the concept of internal protein equilibria (*54*).

In antibodies, these binding equilibria may involve residues that are not in immediate contact with the antigen, the so-called second sphere residues, water molecules, and even distant contacts that define the positions and interactions of the variable domains. This mechanism should be taken into account by antibody engineers when attempting to improve the affinity and/or shift the antibody−antigen contact residues. Introduced point mutations might affect the architecture and the malleability of the binding site, causing cumulative effects. An interesting study published by the Pluckthun group (*55*) shows that a 12 amino acid long peptide with unordered solution structure can be folded into an almost perfect α-helix upon its binding to the antibody. Using directed *in vitro* evolution and ribosome display technology, the authors were able to improve the affinity of this antibody by introducing several mutations predominantly in the second sphere residues that resulted in subtle changes of the geometry of the binding groove affecting the flexibility of the CDRs and the domain orientations. Similar effects were also observed in the affinity maturation study of the anti-fluorescein single chain antibody 4-4-20, which contains a pocket-type binding site (*56*).

In conclusion, measuring the diffusion rates using FCS provides an excellent tool for studying binding interactions. For protein systems similar to the antibody−peptide pairs described in this study, FCS can serve as the ultimate

experimental technique. Monoclonal antibodies 106.3 and BC203 demonstrate high affinities to BNP and bind two distant epitopes, forming robust antibody sandwiches. Both antibodies are used in Abbott diagnostic assays on AxSYM, IMx, and Architect platforms.

ACKNOWLEDGMENT

We thank our colleagues Reika Campbell and Peggy Tsatsos who helped to perform mass-spectrometric analysis and Robynn O'Hare who purified mAb 106.3. We also thank Bryan Tieman for pointing us to the alanine scanning mutagenesis tool and Joan Tyner for discussions of the epitope screening strategies. We express many thanks to Jessie Shih, David Daghfal, and Matt Matias for their support and discussions of the clinical role of BNP and possible configurations of a diagnostic test and to Monique Paricharttanakul for her helpful discussions of the competitive binding models. We are very grateful to Kenton Longenecker and Professor Allen Edmundson for their discussions of antibody binding site architecture; it was Allen's advice to check for the "scorpion tail" effect in the *C*-terminus of BNP. Support that Walt Keirans and Robert Doss provided for this project cannot be overvalued.

REFERENCES

1. Nakao, K., Ogawa, Y., Suga, S., and Imura, H. (1992) Molecular biology and biochemistry of the natriuretic peptide system. I: Natriuretic peptides, *J. Hypertens. 10*, 907−12.
2. Sudoh, T., Kangawa, K., Minamino, N., and Matsuo, H. (1988) A new natriuretic peptide in porcine brain, *Nature 332*, 78−81.
3. Saito, Y., Nakao, K., Itoh, H., Yamada, T., Mukoyama, M., Arai, H., Hosoda, K., Shirakami, G., Suga, S., Minamino, N., and et al. (1989) Brain natriuretic peptide is a novel cardiac hormone, *Biochem. Biophys. Res. Commun. 158*, 360−368.
4. Currie, M. G., Geller, D. M., Cole, B. R., Boylan, J. G., YuSheng, W., Holmberg, S. W., and Needleman, P. (1983) Bioactive cardiac substances: potent vasorelaxant activity in mammalian atria, *Science 221*, 71−73.
5. de Bold, A. J., Borenstein, H. B., Veress, A. T., and Sonnenberg, H. (1981) A rapid and potent natriuretic response to intravenous injection of atrial myocardial extract in rats, *Life Sci. 28*, 89−94.
6. Sonnenberg, H., Cupples, W. A., de Bold, A. J., and Veress, A. T. (1982) Intrarenal localization of the natriuretic effect of cardiac atrial extract, *Can. J. Physiol. Pharmacol. 60*, 1149−1152.
7. Sudoh, T., Minamino, N., Kangawa, K., and Matsuo, H. (1990) C-type natriuretic peptide (CNP): a new member of natriuretic peptide family identified in porcine brain, *Biochem. Biophys. Res. Commun. 168*, 863−870.
8. Chinkers, M., Garbers, D. L., Chang, M. S., Lowe, D. G., Chin, H. M., Goeddel, D. V., and Schulz, S. (1989) A membrane form of guanylate cyclase is an atrial natriuretic peptide receptor, *Nature 338*, 78−83.
9. Ogawa, H., Qiu, Y., Ogata, C. M., and Misono, K. S. (2004) Crystal structure of hormone-bound atrial natriuretic peptide receptor extracellular domain: rotation mechanism for transmembrane signal transduction, *J. Biol. Chem. 279*, 28625−28631.
10. He, X., Chow, D., Martick, M. M., and Garcia, K. C. (2001) Allosteric activation of a spring-loaded natriuretic peptide receptor dimer by hormone, *Science 293*, 1657−1662.
11. Maack, T., Suzuki, M., Almeida, F. A., Nussenzveig, D., Scarborough, R. M., McEnroe, G. A., and Lewicki, J. A. (1987) Physiological role of silent receptors of atrial natriuretic factor, *Science 238*, 675−678.
12. Cohen, D., Koh, G. Y., Nikonova, L. N., Porter, J. G., and Maack, T. (1996) Molecular determinants of the clearance function of type C receptors of natriuretic peptides, *J. Biol. Chem. 271*, 9863−9869.
13. Maekawa, K., Sudoh, T., Furusawa, M., Minamino, N., Kangawa, K., Ohkubo, H., Nakanishi, S., and Matsuo, H. (1988) Cloning and sequence analysis of cDNA encoding a precursor for porcine brain natriuretic peptide, *Biochem. Biophys. Res. Commun. 157*, 410−416.
14. Holmes, S. J., Espiner, E. A., Richards, A. M., Yandle, T. G., and Frampton, C. (1993) Renal, endocrine, and hemodynamic effects of human brain natriuretic peptide in normal man, *J. Clin. Endocrinol. Metab. 76*, 91−96.
15. Suttner, S. W., and Boldt, J. (2004) Natriuretic peptide system: physiology and clinical utility, *Curr. Opin. Crit. Care 10*, 336−341.
16. Woods, R. L. (2004) Cardioprotective functions of atrial natriuretic peptide and B-type natriuretic peptide: a brief review, *Clin. Exp. Pharmacol. Physiol. 31*, 791−4.
17. Colucci, W. S. (2001) Nesiritide for the treatment of decompensated heart failure, *J. Card. Failure 7*, 92−100.
18. Yoshimura, M., Yasue, H., and Ogawa, H. (2001) Pathophysiological significance and clinical application of ANP and BNP in patients with heart failure, *Can. J. Physiol. Pharmacol. 79*, 730−735.
19. Sagnella, G. A. (1998) Measurement and significance of circulating natriuretic peptides in cardiovascular disease, *Clin. Sci. (London) 95*, 519−529.
20. Suzuki, S., Yoshimura, M., Nakayama, M., Mizuno, Y., Harada, E., Ito, T., Nakamura, S., Abe, K., Yamamuro, M., Sakamoto, T., Saito, Y., Nakao, K., Yasue, H., and Ogawa, H. (2004) Plasma level of B-type natriuretic peptide as a prognostic marker after acute myocardial infarction: a long-term follow-up analysis, *Circulation 110*, 1387−1391.
21. Silver, M. A., Maisel, A., Yancy, C. W., McCullough, P. A., Burnett, J. C., Jr., Francis, G. S., Mehra, M. R., Peacock, W. F. t., Fonarow, G., Gibler, W. B., Morrow, D. A., and Hollander, J. (2004) BNP Consensus Panel 2004: A clinical approach for the diagnostic, prognostic, screening, treatment monitoring, and therapeutic roles of natriuretic peptides in cardiovascular diseases, *Congestive Heart Failure 10*, 1−30.
22. Inooka, H., Kikuchi, T., Endo, S., Ishibashi, Y., Wakimasu, M., and Mizuta, E. (1990) Conformation in solution of porcine brain natriuretic peptide determined by combined use of nuclear magnetic resonance and distance geometry, *Eur. J. Biochem. 193*, 127−134.
23. Craik, D., Munro, S., Nielsen, K., Shehan, P., Tregear, G., and Wade, J. (1991) The conformation of porcine-brain natriuretic peptide by two-dimensional NMR spectroscopy, *Eur. J. Biochem. 201*, 183−190.
24. Nielsen, K. J., Barron, P. R., Craik, D. J., Lambert, P. F., and Wade, J. D. (1991) Two-dimensional nuclear magnetic resonance study of brain natriuretic peptide in aqueous solution, *Biochem. Int. 25*, 199−210.
25. Kobayashi, Y., Ohkubo, T., Kyogoku, Y., Koyama, S., Kobayashi, M., and Go, N. (1988) The conformation of alpha-human atrial natriuretic polypeptide in solution, *J. Biochem. (Tokyo) 104*, 322−325.
26. Fairbrother, W. J., McDowell, R. S., and Cunningham, B. C. (1994) Solution conformation of an atrial natriuretic peptide variant selective for the type A receptor, *Biochemistry 33*, 8897−8904.
27. Carpenter, K. A., Wilkes, B. C., De Lean, A., Fournier, A., and Schiller, P. W. (1997) Hydrophobic forces are responsible for the folding of a highly potent natriuretic peptide analogue at a membrane mimetic surface: an NMR study, *Biopolymers 42*, 37−48.
28. Cunningham, B. C., and Wells, J. A. (1989) High-resolution epitope mapping of hGH-receptor interactions by alanine-scanning mutagenesis, *Science 244*, 1081−1085.
29. Tetin, S. Y., and Hazlett, T. L. (2000) Optical spectroscopy in studies of antibody-hapten interactions, *Methods 20*, 341−361.
30. Elson, E. L., Magde, D. (1974) Fluorescence correlation spectroscopy. I. Conceptual basis and theory, *Biopolymers 13*, 1−27.
31. Magde, D., Elson, E. L., and Webb, W. W. (1974) Fluorescence correlation spectroscopy. II. An experimental realization, *Biopolymers 13*, 29−61.
32. Thompson, N. L. (1991) Fluorescence Correlation Spectroscopy, in *Topics in Fluorescence Spectroscopy* (Lakowicz, J. R., Ed.) Vol. 1, pp 337−378, Plenum Press, New York.
33. Rigler, R., and Elson, E. L., Eds. (2001) *Fluorescence Correlation Spectroscopy. Theory and Applications*, Springer-Verlag, Berlin.
34. Foldes-Papp, Z., Demel, U., and Tilz, G. P. (2001) Ultrasensitive detection and identification of fluorescent molecules by FCS: impact for immunobiology, *Proc. Natl. Acad. Sci. U.S.A. 98*, 11509−11514.

35. Tetin, S. Y., Swift, K. M., and Matayoshi, E. D. (2002) Measuring antibody affinity and performing immunoassay at the single molecule level, *Anal. Biochem. 307*, 84−91.
36. Hazlett, T. L., Ruan, Q., and Tetin, S. Y. (2005) Application of fluorescence correlation spectroscopy to hapten-antibody binding, *Methods Mol. Biol. 305*, 415−438.
37. Mishak, R. P., Lim, G. A., Scardina, J. M. (2000) U.S. Patent 6, 162, 902, pp 20, Scios Inc., USA.
38. Tsuji, T., Inouye, K., Yamauchi, A., Kono, M., Igano, K. (2004) U.S. Patent 6, 677, 124 B2, pp 16, Shionogi Seiyaku Kabushiki Kaisha, Japan.
39. King, D. S., Fields, C. G., and Fields, G. B. (1990) A cleavage method which minimizes side reactions following Fmoc solid phase peptide synthesis, *Int. J. Pept. Protein Res. 36*, 255−266.
40. Jiang, J., Dayton, B. D., Brodjian, S. J., and Richardson, P. L. (2005) in *Proceedings of the 8th Chinese International Peptide Symposium*, pp 100−102.
41. Beechem, J. M., Gratton, E., Ameloot, M., Knutson, J., and Brand, L. (1991) The global Analysis of Fluorescence Intensity and Anisotropy Decay Data: Second-Generation Theory and Programs, in *Topics in Fluorescence Spectroscopy* (Lakowicz, J. R., Ed.) pp 241−305, Plenum Press, New York.
42. Hargrove, M. S. (2005) Ligand binding with stopped-flow rapid mixing. *Methods Mol. Biol. 305*, 323−342.
43. Wang, Z. X. (1995) An exact mathematical expression for describing competitive binding of two different ligands to a protein molecule, *FEBS Lett. 360*, 111−114.
44. Nagy, A., Wu, J., and Berland, K. M. (2005) Observation volumes and γ-factors in two-photon fluorescence fluctuation spectroscopy, *Biophys. J. 89*, 2077−2090.
45. Saffarian, S., and Elson, E. L. (2003) Statistical analysis of fluorescence correlation spectroscopy: the standard deviation and bias, *Biophys. J. 84*, 2030−2042.
46. Cunningham, B. C., Jhurani, P., Ng, P., and Wells, J. A. (1989) Receptor and antibody epitopes in human growth hormone identified by homolog-scanning mutagenesis, *Science 243*, 1330−1336.
47. Herron, J. N., He, X. M., Ballard, D. W., Blier, P. R., Pace, P. E., Bothwell, A. L., Voss, E. W., Jr., and Edmundson, A. B. (1991) An autoantibody to single-stranded DNA: comparison of the three-dimensional structures of the unliganded Fab and a deoxynucleotide-Fab complex, *Proteins 11*, 159−175.
48. Tetin, S. Y., Rumbley, C. A., Hazlett, T. L., and Voss, E. W., Jr. (1993) Elucidation of anti-ssDNA autoantibody BV 04-01 binding interactions with homooligonucleotides, *Biochemistry 32*, 9011−9017.
49. Huston, J. S., Margolies, M. N., and Haber, E. (1996) Antibody binding sites, *Adv. Protein Chem. 49*, 329−450.
50. Hunter, C. A., Singh, J., and Thornton, J. M. (1991) Pi-pi interactions: the geometry and energetics of phenylalanine-phenylalanine interactions in proteins, *J. Mol. Biol. 218*, 837−846.
51. Edmundson, A. B., Harris, D. L., Fan, Z. C., Guddat, L. W., Schley, B. T., Hanson, B. L., Tribbick, G., and Geysen, H. M. (1993) Principles and pitfalls in designing site-directed peptide ligands, *Proteins 16*, 246−267.
52. Wyman, J., Jr. (1948) Heme proteins, *Adv. Protein Chem. 4*, 407−531.
53. Wyman, J., Jr. (1964) Linked functions and reciprocal effects in hemoglobin: A second look, *Adv. Protein Chem. 19*, 223−286.
54. Weber, G. (1972) Ligand binding and internal equilibria in proteins, *Biochemistry 11*, 864−878.
55. Zahnd, C., Spinelli, S., Luginbuhl, B., Amstutz, P., Cambillau, C., and Pluckthun, A. (2004) Directed in vitro evolution and crystallographic analysis of a peptide-binding single chain antibody fragment (scFv) with low picomolar affinity, *J. Biol. Chem. 279*, 18870−18877.
56. Midelfort, K. S., Hernandez, H. H., Lippow, S. M., Tidor, B., Drennan, C. L., and Wittrup, K. D. (2004) Substantial energetic improvement with minimal structural perturbation in a high affinity mutant antibody, *J. Mol. Biol. 343*, 685−701.

BI0607047